Understanding and Including the Dynamics of Extreme Natural Hazard Event Uncertainty Within the Overall Offshore Wind Farm Project Risk Assessment Using a Causality-Based Graphical Modelling Approach

Zamora, Rafael; Qin, Jianjun; Kristensen, Anders Schmidt; Mehmood, Saqib; Ahmed, Shakeel; Cuthbert, S.

Published in:
Safety and Reliability - Safe Societies in a Changing World

Publication date:
2018

Document Version
Publisher's PDF, also known as Version of record

Safety and Reliability – Safe Societies in a Changing World – Haugen et al. (Eds)
 ISBN 978-0-8153-8682-7

Understanding and including the dynamics of extreme natural hazard event uncertainty within the overall offshore wind farm project risk assessment using a causality-based graphical modelling approach

R. Zamora, J. Qin, A.S. Kristensen, S. Mehmood & S. Ahmed
Danish Center for Risk and Safety Management, Aalborg University, Esbjerg, Denmark

S. Cuthbert
Ørsted, Fredericia, Denmark

ABSTRACT: Offshore wind structures are subject to the combined action of wind and wave loads. A change of these loads may significantly affect the integrity of the structural elements. Increased instabilities in the Earth's climate system could increase the frequency of extreme events (e.g. rogue waves) well beyond the frequency values currently recommended within structural design standards. Inherent to extreme event modelling is the need to use expert (subjective) judgement and sparse data sets. In this context, a Bayesian Belief Network (BBN) can be applied to describe the effect of these changes on the frequency of rogue waves within wind farms located in shallow water depths of 20–60 metres. This graphical modelling approach provides the structure to effectively communicate, among others, parameter uncertainty, causality across multiple risk factors, quantitative definition of assessment subjectivity or potential impact of a change in rogue wave frequency relative to that described in current design standards.

1 INTRODUCTION

The term "rogue", "freak", "abnormal" or "giant" wave commonly refers to waves that are very steep and large in absolute measures and, at the same time, significantly larger than the surrounding waves in the sea state, and are thus unexpected (Bitner-Gregersen, 2017). They are statistically unlikely to occur in a given sea state (either low, intermediate or high), based on averaged properties of that sea state (Bitner-Gregersen & Gramstad, 2015).

This physical phenomenon is not fully understood, but increasing reliable measurements and records, as well as the significant increase in computational power and numerical modelling capacity, allow to explore these extreme events with greater accuracy.

There are several motivations to reduce the risk of wave-related incidents. First, because they clearly represent a current threat to marine installations. Second, because more severe sea state conditions may be expected in some ocean regions associated with climate change and global warming (IPCC Panel, 2014). Third, because understanding and forecasting waves under various conditions is essential with respect to design and operation of offshore structures.

Based on these initial premises, addressing these extreme events as potential risk and including them in the customary Risk Assessment process of a company that operates physical assets in an offshore environment is entirely justified, despite its complexity and the high number of uncertainties involved.

In the present work a causality-based probabilistic graphical modelling methodology is proposed to assess the risk associated with rogue waves in offshore wind farm projects at the final design stage. The methodology includes the impact of future climate change and provides the structure in which to effectively communicate: a) parameter uncertainty; b) correlation across multiple risk factors (i.e. "Systems of Systems" (SoS) complexity mapping/analyses); c) definition of assessment subjectivity; d) and potential impacts of low probability catastrophic events (i.e. extreme events). The methodology provides a holistic framework that can be integrated into existing decision-making processes currently defined within a large capital project execution process.

In brief, the method studies the probability of a rogue wave impacting an offshore structure situated in a predefined location of the Northern North Sea, between 20 and 60 m depth, and includes 3 main stages: risk understanding, qualitative bow-tie creation; and transformation to a Belief Bayesian Network.

2 RISK UNDERSTANDING

Risk assessment is to a large extent about gaining 'risk understanding' in the sense of knowledge—justified beliefs, by producing a risk description (C_0,Q,K), where C_0 are the specified consequences of the activity studied, Q a measure of uncertainty, and K is the background knowledge on which C_0 and Q are based (Amundrud & Aven, 2015). According to these authors, these justified beliefs are based on data, information (relevant processed data) and models. The uncertainty judgments about C_0 using Q can also be seen as justified beliefs.

K is a limiting aspect in the proposed methodology, due to the lack of understanding of the physical process of creation of rogue waves. For example, describing the wave phenomenon is the result of a set of uncertainties. The random model for ocean waves is constructed by representing the sea surface as a sum of elementary waves with different wavelengths, frequencies, and directions of propagation (Bitner-Gregersen & Gramstad, 2015). However, in reality ocean waves are not described exactly by a linear formulation or second-order theories, and therefore require a set of increasingly accurate formulations. The more accurate, the more mathematically complex and more difficult the model will be. As a result, the logical functions and equations included in the proposed graphical model are based on the linear theory, the most tractable approach for the graphical model under design.

Uncertainty related to environmental phenomena may be divided in aleatory uncertainty (natural randomness) and epistemic (knowledge) uncertainty; and the latest in: data uncertainty, statistical uncertainty, model uncertainty and climatic uncertainty (Bitner-Gregersen et al. 2013).

Assessing data uncertainty is out of the scope of this study, so available data are assumed to be appropriate. To minimize the statistical and climatic uncertainty, a long-term data source was selected. The European Centre for Medium-Range Weather Forecasts' ERA-Interim is a global atmospheric reanalysis from 1979, publicly accessible and continuously updated in real time (European Centre for Medium-Range Weather Forecast, 2017). After establishing a geographical location in the Northern Sea, 4 measurements per day were obtained between 1979 and 2017 (about 55.000 values per variable) for 30 different variables. Only 9 of them were considered relevant for the project: model depth (d), zero-crossing mean period (Tz), wave spectral directional width (σ_θ), significant wave height (Hs), mean wave direction (θ), mean direction of wind waves (θ_1), mean direction of swell (θ_2), and Benjamin-Feir index (BFI).

There are other relevant variables, such as the wave length (λ), that are not independent. In these cases, formulae given by the Recommended Practice DNVGL-RP-C205 have been used (DNV GL, 2017).

Finally, defining and managing the model is the core part of this work and a main responsibility of the risk analyst (designing, building, assigning probability, running simulations, reporting and maintaining). It reflects the limitations of the previous factors and adds new uncertainties, due to failed assumptions in physical process formulations, or choices of probability distribution types for representation of uncertainties. In this regard, the method tries to register and track all the detected uncertainties. To limit this effect, all the variables were fitted to a probability distribution using the software tool, ModelRisk (Vose Software, 2018) only when the best fit was not supported by the Bayesian Network software (OpenBUGS).

3 BOW-TIE CREATION

The bow-tie is a graphical approach frequently used to represent a Risk Event, its Causes (Drivers), Prevention Barriers (Controls), Mitigation Barriers, and its Consequences (Impacts) in a visual and logical manner. Centered on a critical (risk) event, it is composed of a simplified fault tree on the left-hand side and an equally simplified event tree on the right-hand side showing the possible consequences of the critical event based on the failure or success of safety functions (Khakzad et al. 2013). To understand the relations and dependences among factors involved in the creation and impacts of rogue waves and climate change on offshore wind structures, a qualitative bow-tie is proposed. The first step consists of formulating the critical event: impact of a breaking rogue wave on an offshore wind structure (named "IMPACT" in the graphical model). This step seems to be obvious, but in complex or emerging risks it is essential to organize and plan the following phases of the method.

In this case, due to the complexity of the analyzed physical phenomena, the bow-tie focuses on the left-side, or analysis of causes (drivers) and barriers (controls). The event tree of consequences is reduced to one: the failure of the structure (F).

After a deep review of the state-of-the-art related to rogue waves and climate change impacts on the study area, as well as the available data, the drivers and controls are analyzed individually and placed in the bow-tie, establishing the appropriate connections and causal relations. The graphic is continuously updated until it gets its final shape, shown in Figure 1.

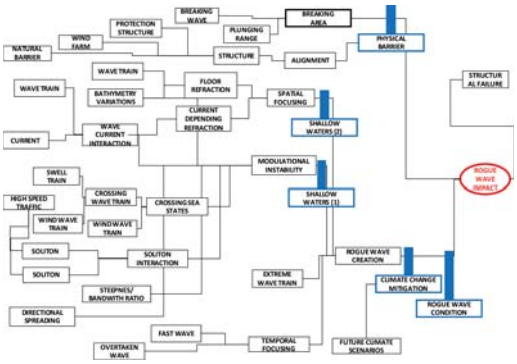

Figure 1. Final bow-tie.

Several different mechanisms may be responsible for generating rogue waves such as linear focusing of energy (spatial and dispersive: K_f, K_c and T_f), wave-current interactions (CI), crossing seas (wind sea and swell or two swell systems, CS), quasi-resonant nonlinear interactions (modulational instability, BFI), shallow water effects (SWC_i), solitons interactions (SO), directional spreading (DS), and wind forcing (W).

Atmospheric forcing has not been considered in the bow-tie as a cause of waves to simplify the visual understanding of the process. The relevant variables obtained from the dataset are included in the bow-tie as primary events. Other relevant variables, as slope (SL), angle between the wave crest and depth contours (α_0), angle between target and protection structure (β), Ursell number (U_R) or maximum height (H_m) are added as primary events, when statistical data are not available but are required for a consistent explanation of an intermediate event. Some of them are calculated in future steps or treated as assumptions. The bow-tie shows two main controls: protective structure (O), as a physical barrier to avoid the impact of a breaking rogue wave against the offshore wind structure (OWS); and climate change (C). C is placed as control, assuming its barrier effect is focused on limiting or preventing the CO_2 emissions caused by humans, where the key assumption is that the accumulation of CO_2 and other greenhouse gases are the primary drivers for climate change and that the human population is largely the driver for the significant increase in the atmospheric concentrations of those gases in the past 200 years. Other controls are related to shallow water restrictions or used for reversing interactions of separated subsystems (current, ship traffic, etc.) over the wave fields or between drivers of different nature, when needed. The other three are natural controls: shallow water conditions and rogue wave conditions.

4 BAYESIAN NETWORK

The bow-tie graphical model is used in this method as a primary tool to understand the risk and locate the critical event in its cause-effect framework. However, it presents a static picture of the problem. Besides, no causal relation can be established between primary events or other events of different branches of the fault or event tree. These problems are solved with its transformation to a Belief Bayesian Network (BBN).

A BBN is an explicit description of the direct dependencies between a set of variables, in the form of a directed graph and a set of nodes linked to a probability. This structure offers the following benefits (Fenton & Neil, 2013): modelling causal factors explicitly, reasoning from effect to cause and vice versa; updating the probability distributions for every unknown variable whenever an observation is entered into any node; reducing the burden of parameter acquisition; overturning previous beliefs in the light of new evidence (explaining away); making predictions with incomplete data; combining diverse types of evidence including both subjective beliefs and objective data; and arriving at decisions based on visible, auditable reasoning.

The conversion of a bow-tie into a BBN is summarized in Figures 2 and 3.

The BBN includes different interacting systems besides the waves system, and includes the current, seabed, wind, climate, ship traffic and artificial structure. Figure 4 shows this graphical model.

The fitted distributions are included as parent nodes, because are the basic parameters of the model. There are 13 "parent distributions", whereas only four of them are not obtained from available data. In these cases, a uniform distribution is assumed. One variable relies on the seabed conditions and would be subject to a better characterization with the consideration of a bathymetry

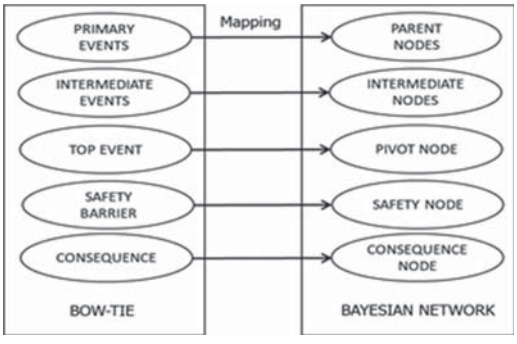

Figure 2. Mapping algorithm from bow-tie to Bayesian Network (Khakzad et al., 2013).

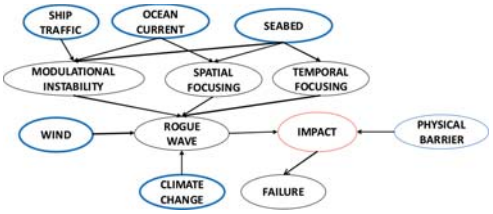

Figure 3. Bayesian Network related to bow-tie elements.

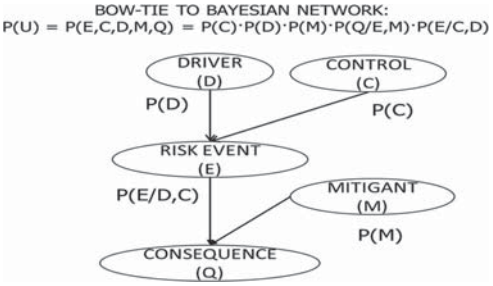

Figure 4. Overall Bayesian Network with interacting systems.

model: the angle between wave crests and depth contours (α_0). Another one (Froude Number Fd) depends on the ship traffic around the offshore wind turbine structure (OWS), but its assessment is out of the scope of this work.

Following the conclusions of the bow-tie analysis, the failure of the OWS occurs when a rogue wave impacts on it. The probability of this impact is "*the probability of a rogue wave breaking in front of the OWS within the plunging range without a protective structure in between*". When the wave breaks just at the location or behind, the plunge distance is not relevant for the targeted OWS. By contrast, when the wave breaks in front of the structure, this distance is relevant, because it defines the area where the wave is dangerous. However, given that the available data are restricted to the selected location, further spatial considerations (i.e. defining a breaking point or a plunge distance in front of the OWS) are out of the scope of this study.

Therefore, for this event to happen or not, it is necessary the presence of a rogue wave that breaks without an opposing protective structure in between.

In the graphical model, an extreme wave is considered a rogue wave R when the height doubles the significant height H_s ($R > 2H_s$) (Bitner-Gregersen & Gramstad, 2015). The wave height is limited by breaking. The maximum wave height H_b condition is based on the Recommended Practice DNVGL-RP-C205 (DNV GL, 2017):

$$H_b = \lambda 0.142 tanh \frac{2\pi d}{\lambda} \quad (1)$$

where λ is the wave length corresponding to water depth d.

The accompanying structure may be natural or artificial. If the structure is artificial, it can be either of floating type with a mooring to the seafloor or a solid anchored structure that is submerged or slightly above the surface. In an offshore wind farm, another OWS may protect the selected structure from the impact of a rogue wave. The condition to be protective is being total or partially aligned with the OWS in the mean wave direction. This condition happens, as shown in Figure 5, when the angle between the wave and the segment that links both structures (β) is between θ+90º and θ+270º (no other physical phenomena, i.e. refraction or diffraction, are included).

The critical assumption of the model is that the extreme wave heights (H_m) calculated from the available data are generated exclusively by the wave focusing under the action of wind. The final wave height (W) is then the result of an increase over the value of H_m due to the causes explained through the bow-tie, as expressed in Eq. (2):

$$W = H_m \cdot (1+C_{5\,m} \cdot SWC_1 \cdot M + C_{6l} \cdot C + step\,(0.6-U_R) \cdot C_{7t} \cdot TF + C_{3f} \cdot SWC_2 \cdot step\,(K_f-1) \cdot (K_f-1) + C_{1c} \cdot step\,(CI) \cdot K_c) \quad (2)$$

where

H_m = extreme value of height;

K_c = height increase proportion due to current refraction;

K_f = height increase proportion due to floor refraction;

M = height increase proportion due to modularity;

C = height increase proportion due to the climate change; and

TF = height increase proportion due to temporal focusing.

It may be argued that the measured heights are already the result of these causes or, at least, the

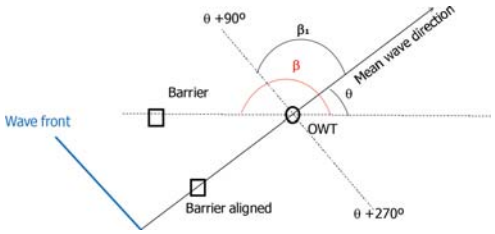

Figure 5. Alignment of the protective structure.

linear causes, i.e. spatial and temporal focusing. To deal with such complications, each driver has one control node (constant), so that the unexpected cause or interacting system can be eliminated from the model: C_{1c} for the current; C_{2s} for the ship traffic; C_{3f} for the seabed refraction; C_{4o} for the protective structure; C_{5m} for the modularity instability; and C_{6t} for the temporal focusing.

There are also natural controls (step(0.6-U_R), step(CI), SWC1, SWC2) that cancel the drivers due to natural conditions. These natural conditions can be modelled.

Only height increases are considered, so the condition to take refraction into account is K_f >1: step (K_f – 1).

H_m is calculated following the extreme value theory and fitting the results to a Gumbel distribution.

K_f is calculated based on the Recommended Practice DNVGL-RP-C205 (DNV GL, 2017):

$$K_f = K_s \cdot K_r \tag{3}$$

$$K_r = \left[\frac{1 - sin^2\alpha_0 tanh^2(kd)}{\cos^2\alpha_0}\right]^{-1/4} \tag{4}$$

$$K_s = \sqrt{\frac{c_{g,0}}{c_g}} \tag{5}$$

where

K_s = shoaling coefficient;

K_r = refraction coefficient;

α_0 = the angle between the wave crest and the depth contours at the location;

k = wave number;

d = depth; and

C_g = group velocity.

K_c is a good example of the difficulties found to model some of the drivers involved in the process. The first approach to define the variable K_c was based on the analysis of this phenomenon presented by Sorensen (Sorensen, 2006). Figure 6

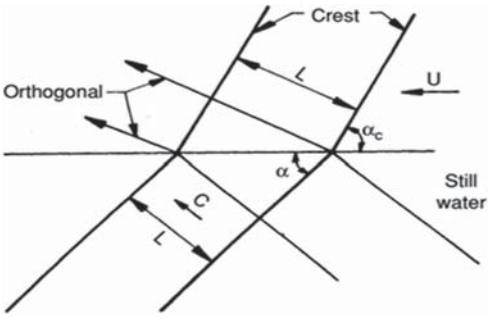

Figure 6. Definition sketch for wave refraction by a current (Sorensen, 2006).

shows how a wave propagating with speed C from still water to water having a current velocity U, changes its direction.

In mathematical terms, these equations are obtained:

$$K_c = \frac{H_c}{H} = \left(\frac{L_c}{L}\right)^2 \frac{cos\alpha}{cos\alpha_c}\left[\frac{\left(1 - \frac{U}{C}sin\alpha\right)^6}{1 + \frac{U}{C}sin\alpha}\right] \tag{6}$$

$$L_c = L\frac{sin\alpha_c}{sin\alpha} \tag{7}$$

$$sin\alpha_c = \frac{sin\alpha}{\left(1 - \frac{U}{C}sin\alpha\right)^2} \tag{8}$$

where

H_c = Height after refraction;

H = Height before refraction;

L_c = Wave length after refraction;

L = wave length before refraction;

U = current velocity;

C = wave velocity;

α = angle between the current and the crest front;

α_c = angle between the current and the crest front after refraction.

Considering $K_c = H_c/H$, an expression of K_c as function of α and α_c can be obtained, but introducing it in the model was impossible and always led to a systematic software error. Other equations were checked, such as those presented by Iwagaki et al. (1977). A different approach was finally selected based on the work by Mathiesen (1987), which is derived from the computer model to measure the refraction of ocean directional wave spectra and applied it to a circular current whirl typical in the Norwegian coastal current. This model found that the relative changes in wave heights were within ±20% as compared with the wave height of the incoming waves.

M is calculated as the average probability of the nonlinear modularity drivers, which are: solitons interactions (SO), variable bathymetry (SL), crossing seas (CS), Benjamin-Feir interaction (BFI), directional spreading (DS) and wave-current interaction (CI). M is limited to a maximum value (M_{max}) of 0.20. This value is defined considering several systematic studies which shows that effects of modulational instability can enhance the crest height for long-crested waves by up to 20%, at lower probability levels, while the troughs become about 20% deeper than second–order troughs (Kharif et al. 2009).

C is calculated based on the CO_2 emissions originating from the socio-economic scenarios (A1B, A2, B1 and B2) proposed by The Intergovernmental

Panel on Climate Change IPCC and the values of emissions currently estimated for the North Sea.

T_f is calculated as a function of the Ursell number U_R, with a maximum value to be established at the moment:

$$U_R = \frac{H\lambda^2}{d^3} \tag{9}$$

Kharif et al. (2009) stated that this number characterizes the ratio of nonlinearity to dispersion. When the Ursell parameter is small, the nonlinearity can be neglected, and the wave is a linear dispersive wave. In real situations of wind waves, the values of U_R parameters are not too large, and the dispersive trains contribute significantly to the statistical wave characteristics. Based on these authors, a value of $U_R < 0.6$ is selected to consider the impact of the temporal focusing as relevant.

There are two restrictions related to the shallow waters which must be considered, and are given the variable names, SWC_1 and SWC_2. Water is considered shallow when the surface waves are noticeably affected by bottom topography (Bitner-Gregersen & Gramstad, 2015). This condition occurs when the depth, d, becomes less than half the wavelength, λ.

Modulational instability becomes weaker with decreasing depth and it is suspected to play a less important role in shallow water (Bitner-Gregersen & Gramstad, 2015). Benney & Roskes (1969) estimated that modulational instability disappears when $2\pi d/l < 1.363$ for unidirectional waves. Under this threshold, the model cancels the driver M. This is the restriction with the variable name, SWC_1

Similarly, the seabed related refraction (K_f) is canceled when the shallow water condition is not accomplished (restriction SWC_2).

4.1 *Modulational instability drivers*

Seven drivers are involved in the creation of nonlinear instability. Their inclusion, conditions and limits are discussed in the following sections.

4.1.1 *Solitons interaction (SO)*

Solitons interaction has been suggested as a source of nonlinearity in shallow water (Kharif et al., 2009). Peterson et al. (2003) linked this mechanism to relatively shallow coastal areas with high ship traffic density, particularly high-speed ships when they sail with critical or supercritical speeds. These speed levels rely on a value of the Froude number, F_d, which is the ratio of the ship speed and the maximum phase speed of gravity waves, equal or higher than 1. Therefore, the model constrains the impact of this driver to this threshold. It is out of scope of this study to analyze the traffic in the vicinity of the location, so a uniform distribution has been used for the variable F_d.

4.1.2 *Variable bathymetry (SL)*

Recent works have shown that the probability of rogue waves may increase on the shallow side of an underwater slope. Sergeeva et al. (2011) linked the probability of rogue waves to the wave steepness, which is characterized in terms of the Ursell parameter. Both variables increase when the depth decreases (water shallowing), and the wave state deviates from the Gaussian. Based on previous research, the condition for nonlinearity due to the interactions with a variable bottom has been fixed when $U_R > 0.6$ (Kharif et al., 2009).

4.1.3 *Crossing seas (CS)*

When two wave systems (wind sea and swell or two swell systems) are separated in direction or frequency and cross, the modularity increases depending on the angle between them. Both wave trains are assumed to be narrow banded and weakly nonlinear (Kharif et al., 2009).

Onorato et al. (2010) suggested that an increased probability of rogue waves was associated with angles between 40° and 60°. This is the condition used in the graphical model. ERA INTERIM database offers separated information about the mean wind waves directions (θ_1) and mean swell direction (θ_2), so the possibility of crossing wind seas is not considered.

4.1.4 *Benjamin-Feir interaction (BFI)*

A key parameter controlling the importance of the nonlinear wave-wave interactions is the Benjamin–Feir Index (BFI) which is the ratio of the wave steepness to the spectral bandwidth (Kharif et al., 2009).

$$BFI = \frac{\varepsilon\sqrt{2}}{\delta_\theta} \tag{10}$$

where:

ε = wave steepness; and

δ_θ = spectral directional width.

Instability condition is given by Eq. (11), and is used as a condition in the graphical model (Bitner-Gregersen, 2017):

$$\sqrt{2}BFI > 1 \tag{11}$$

4.1.5 *Directional spreading (DS)*

Onorato et al. (2002) showed that the probability of occurrence of rogue waves depends not only on BFI, but also on the directional spreading of the waves. Waseda et al. (2011) found evidence that occurrence of rogue waves was associated with sea states with directional spreading of less than about 30°, sug-

gesting that sea states with increased occurrence of rogue waves may occur in realistic ocean conditions. This has been the condition used in the model.

4.1.6 *Nonlinear wave-Current Interaction (CI)*

There are theoretical, experimental, and numerical evidences to support that in some situations the combined effect of wave nonlinearity and currents can lead to an increase in rogue wave occurrence (Nakicenovic et al., 2000). Janssen & Herbers (2009) first discovered that initially stable narrow banded wave fields could become unstable when the nonlinearity was increased due to linear focusing. Toffoli et al. (2015) experimentally showed that realistic random waves propagating in opposing currents could destabilize, with a resulting increase in the occurrence of rogue waves, even for waves with directional spread that normally obey near-Gaussian properties. The probability of a current opposing to a wave field depends then on the angle between wave and current. The opposing condition is addressed by the model as the probability of the mean current direction (θc) between the values of θ + 90º and θ + 270º, with a maximum when θc is equal to θ + 180º, as shown in the Figure 7.

4.2 *Addressing climate change*

For the estimation of the climate change impact on the frequency of occurrence of a breaking rogue wave within the location proposed for an offshore wind farm, several assumptions have been made. It is accepted that there is a stochastic dependence between levels of CO_2 in the atmosphere and the ocean wave climate. On the other hand, only CO_2 is considered as a factor of climate change, although it is just one of the components of the greenhouse gas group (GHG).

The projections of future climate change scenarios are based on the four marker scenarios (A1B, A2, B1 and B2) proposed by The Intergovernmental Panel on Climate Change IPCC, over the twenty-first century (Quante & Colijn, 2016). Each emission scenario reflects different assumptions on future socioeconomic development. Scenario A2 is the worst, followed by A1, B2 and B1.

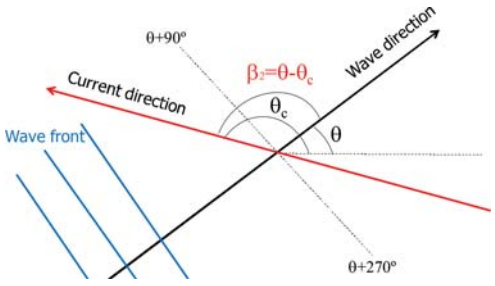

Figure 7. Wave-current interaction.

Regarding the study area, Grabemann et al (2015) analyzed a set of ten wave climate to estimate the possible impact of anthropogenic climate change on mean and extreme wave conditions in the North Sea. The projections were based on different IPCC emission scenarios, included different global and regional models starting from different initial conditions.

They found a solid pattern for the increase in median and severe significant wave height in the eastern North Sea (parts of the southeastern North Sea and large parts of the Dutch, German, and Danish coasts up to the Skagerrak) towards the end of the twenty-first century, while a decreasing trend in the western North Sea was detected. However, the magnitude of this increase was much more uncertain and oscillates between about –10 and 15% relative to the reference Hs. These numbers are consistent with other relevant studies in the area, which establish the increase between 6–8%, or up to 10% (Kharif et al., 2009).

Therefore, in the model the increase on the wave height has been defined as:

$$C = c_0 \cdot \sum_j^{10} x_{ij} \cdot s_i \tag{12}$$

where c_0 = maximum emission factor in decimal fraction; x_{ij} = reduction factor for the emission scenario i during the decade j in decimal fraction; and s_j = emission scenario.

Based on the abovementioned data, a value of 0.10 has been assigned to c_o. It corresponds to the value for the worst scenario (A2). The values of s_{ij} have been calculated based on the projections of the IPCC simulated with model AIM in the OCDE region, as stated in Table 1.

Table 1. Emission Reduction factors based on IPCC scenarios (x_{ij}).

Decade	Scenario s_i			
	A2	A1	B2	B1
1990	1	1	1	1
2000	1	1	1	1
2010	1	0.97	0.93	0.89
2020	1	0.91	0.86	0.81
2030	1	0.83	0.78	0.71
2040	1	0.77	0.73	0.64
2050	1	0.72	0.68	0.58
2060	1	0.64	0.58	0.48
2070	1	0.57	0.49	0.4
2080	1	0.49	0.41	0.31
2090	1	0.4	0.33	0.23
2100	1	0.32	0.26	0.16

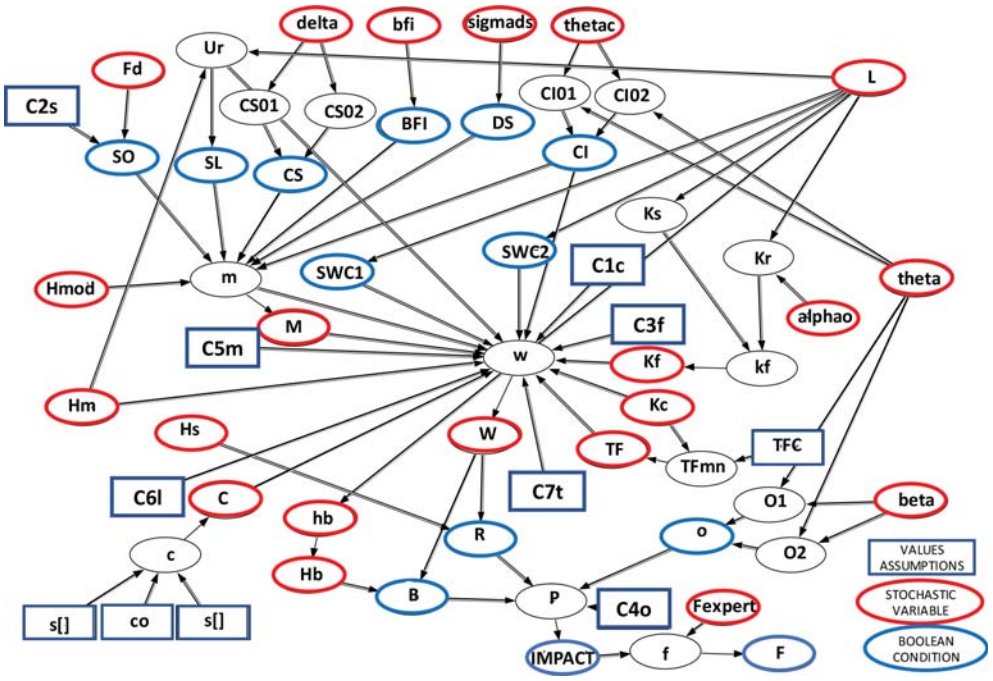

Figure 8. Final version of the Bayesian Network.

The final structure of the proposed Bayesian Network is presented in Figure 8.

5 DISCUSSION AND CONCLUSIONS

In the current study, a method for assessing a complex risk associated to physical phenomena not fully understood has been presented. The high level of complexity results in a high number of uncertainties which necessarily must be faced by the risk analyst. The focus of this study has been on understanding the physics behind the rogue wave phenomenon and determining the conditions under which such waves can be expected to occur more frequently when considering specific temporal and spatial ranges. Without the right outcome from this stage, the aim at creating a Bayesian Network would have been impossible. The role of the analyst in a decision-making process is to create a model as efficient as possible. This requirement includes its running speed, computational calculation and memory requirements, maintenance effort, file size, the least amount of assumptions, and finally, the ability to communicate the risk and the utility for the decision makers.

Due to the complexity of the risk analyzed, the number of assumptions in the model is remarkable, but a considerable effort has been made to manage those assumptions via: tracking for awareness and future improvement; and defining the model with multiple options for isolating and simulating only a partial number of individual drivers.

Currently, the BNN is being tested under different scenarios and limitations. Further conclusions will arise with the coming analysis of the results. In the worst scenario, the method will serve as a learning tool to understand the risk and its consequences in a deeper way. It will also be used to perform sensitivity analysis of the different drivers involved in the critical event. The optimal implementation would be reached when the model is used as a part of the strategic decision-making process. However, several limitations have been already detected. The output interface of the BBN software (OpenBUGS) complicates the presentation of results. There are other products in the market that seem to be more prepared for sharing results with the management in a visual way. On the other hand, spatial considerations cannot be addressed by the graphical model, i.e., the analysis of the plunging distance and the location of a potential breaking point of the wave in front of the structure.

REFERENCES

Amundrud, O., & Aven, T. (2015). On how to understand and acknowledge risk. *Reliability Engineering and System Safety*, 142, 42–47.

Benney, D.J., & Roskes, G.J. (1969). Wave Instabilities. Studies in *Applied Mathematics*, 48(4), 377–385.

Bitner-Gregersen, E. (2017). Rethinking rogue waves. Towards better modelling, insight and action. DNV. GL.

Bitner-Gregersen, E., & Gramstad, O. (2015). Rogue waves. Impact on ships and offshore structures. DNV GL STRATEGIC RESEARCH & INNOVATION POSITION PAPER 05–2015.

Bitner-Gregersen, E.M., Eide, L.I., Hørte, T., & Skjong, R. (2013). Ship and Offshore Structure Design in Climate Change Perspective.

DNV GL. (2017). Edition August 2017 Environmental conditions and environmental loads. Recommended practice DNVGL-RP-C205 (August 201).

European Centre for Medium-Range Weather Forecast. (2017). Who we are | ECMWF. Retrieved 15 December 2017, from https://www.ecmwf.int/en/about/who-we-are.

Fenton, N., & Neil, M. (2013). *Risk Assessment And Decision Analysis with Bayesian Networks.* CRC Press Taylor & Francis Group.

Grabemann, I., Groll, N., Möller, J., & Weisse, R. (2015). Climate change impact on North Sea wave conditions: a consistent analysis of ten projections. *Ocean Dynamics*, 65(2), 255–267.

IPCC Panel. (2014). Climate Change 2014: Synthesis Report.

Iwagaki, Y., Sakay, T., Tsuda, T., & Oka, Y. (1977). Wave refraction and wave height variation due to current. Bulleting of the Disaster Prevention Research Institute, 27(2), 73–91.

Janssen, T.T., & Herbers, T.H.C. (2009). Nonlinear Wave Statistics in a Focal Zone. J*ournal of Physical Oceanography,* 39(8), 1948–1964.

Khakzad, N., Khan, F., & Amyotte, P. (2013). Dynamic safety analysis of process systems by mapping bow-tie into Bayesian network. *Process Safety and Environmental Protection*, 91(1–2), 46–53.

Kharif, C., Pelinovsk, E., & Slunyaev, A. (2009). Rogue Waves in the Ocean. Springer.

Mathiesen, M. (1987). Wave refraction by a current whirl. Journal of Geophysical Research: Oceans, 92(C4), 3905–3912.

Nakicenovic, N., Alcamo, J., Davis, G., De Vries, B., Fenhann, J., Gaffin, S., … others. (2000). Emissions scenarios.

Onorato, M., Osborne, A., & Serio, M. (2002). Extreme wave events in directional, random oceanic sea states. P*hysics of Fluids,* 14(4), L25–L28.

Onorato, M., Proment, D., & Toffoli, A. (2010). Freak waves in crossing seas. T*he European Physical Journal-Special Topics*, 185(1), 45–55.

Peterson, P., Soomere, T., Engelbrecht, J., & Groesen, E. Van. (2003). Soliton interaction as a possible model for extreme waves in shallow water. Nonlinear Processes in *Geophysics*, 10, 503–510.

Quante, M., & Colijn, F. (2016). North Sea Region Climate Change Assessment. SpringerOpen.

Sergeeva, A., Pelinovsky, E., & Talipova, T. (2011). Nonlinear random wave field in shallow water: variable Korteweg-de Vries framework. *Natural Hazards and Earth System Sciences,* 11(2), 323–330.

Sorensen, R.M. (2006). *Basic Coastal Engineering* (3rd ed., p. 331). Boston: Springer.

Toffoli, A., Waseda, T., Houtani, H., & Cavaleri, L. (2015). Rogue waves in opposing currents: an experimental study on deterministic and stochastic wave trains. *Journal of Fluid Mechanics*, 769, 277–297.

Vose Software. (2018). Risk Analysis Software for Excel | Vose Software. Retrieved 13 January 2018, from https://www.vosesoftware.com/products/modelrisk/.

Waseda, T., Hallerstig, M., Ozaki, K., & Tomita, H. (2011). Enhanced freak wave occurrence with narrow directional spectrum in the North Sea. Geophysical Research Letters, 38(13).